Available online at www.sciencedirect.com
SCIENCE DIRECT
Cement and Concrete Research 36 (2006) 1304–1311
Cement and Concrete Research

On the relationship between pore structure and chloride diffusivity from accelerated chloride migration test in cement-based materials

C.C. Yang *

Institute of Materials Engineering, National Taiwan Ocean University, Keelung 202, Taiwan, ROC

Received 10 February 2005; accepted 9 March 2006

Abstract

In this study the electrochemical technique is applied to accelerate chloride ion migration in concrete to determine the chloride ions in anode cell, and the pore characteristic of the same mortars in concrete was obtained from the mercury intrusion porosimetry (MIP). The plain ordinary Portland cement and the constant aggregate with eight w/c ratios ranging from 0.3 to 0.65 were used. A good linear relationship between the steady-state migration coefficient and non-steady-state migration coefficient based on the same experimental setup and specimens was obtained. Both of the steady-state migration coefficient and non-steady-state migration coefficient were linearly related to the capillary pore volume and the critical pore diameter.

Keywords: Chloride migration coefficient; Steady-state; Non-steady-state; Mercury intrusion porosimetry; Capillary pore

1. Introduction

The pore structure of cement-based materials is one of its most important characteristics and strongly influences both its mechanical behavior and its transport properties. The durability of cement-based materials depends on their transport properties, and it is affected by the pore structure.

Cement-based materials contain air voids, capillary pores, and gel pores (the interlayer spaces in a C–S–H gel), and the pores in concrete are randomly sized, arranged, and connected [1]. Because of the wide range of feature sizes in pore, from nanometer-sized pores to micrometer-sized air voids [2], the microstructure of cement paste is very complex. The mercury intrusion porosimetry (MIP) is the most widely used method for the study of pore structure characteristics of cement-based materials. The MIP method has been used to investigate the influence of mineral admixture effect on the pore structure [3–9] and the effects of carbonation on pore structure and diffusion properties [10]. Halamickova et al. [11] found that the coefficient of chloride ion diffusion varied linearly with the critical pore radius as determined by the MIP, and the permeability followed a power–law relationship vs. the critical radius. However, there are some limitations of the MIP testing in determining pore size distributions in cement-based materials. The very fine pores in diameters from 1 to 3 nm are not intruded by mercury for most commercial porosimeters [12]. Using image analysis, Diamond [12] found that the pore shapes in hydrated cements are different from cylindrical pores assumed by the Washburn equation model. The assumptions in the Washburn equation model influences the result of pore size distribution in cement-based materials measured with the MIP. The "ink bottle" effect [12,13] and the segmentation of capillary pores by the gel [12] produce the overestimation of fine pores and for the underestimation of larger capillary pores. During mercury intrusion under very high pressures, the mercury breaks down fragile walls within the cement microstructure [13,14]. Diamond [12] pointed out that the MIP measurements are useful only to provide threshold diameters and intrudable pore space measurements, which can serve as comparative indices for the connectivity and capacity of the pore system in hydrated cements.

In order to accelerate the movement of chloride ions, several accelerated chloride ions diffusion test methods by the application of an electrical field [15–19] were developed. The

* Fax: +886 2 2462 5324.
E-mail address: ccyang@mail.ntou.edu.tw.

0008-8846/$ - see front matter © 2006 Elsevier Ltd. All rights reserved.
doi:10.1016/j.cemconres.2006.03.007

test ASTM C1202 (RCPT) [15], the current passing through the concrete specimens in 6 h is measured, and the resistance of the concrete to chloride ion penetration is assessed by the total charge passed in non-steady-state [20]. Feldman et al. [21,22] have shown a good correlation between 6 h charge passed obtained from RCPT and both initial current and the conductivity of concrete measured at the beginning of the test, and pointed out that measurements of initial current or conductivity provides a rapid and cheap way of predicting concrete chloride permeability. Using the total charge passed during the last 24 h before the termination of the test to define the final coulomb value from steady-state chloride migration test, Sugiyama et al. [23] found that the final coulomb was linearly related to the concrete migration coefficients. Truc et al. [24] presented a method for measuring the chloride diffusion coefficient from a steady-state test by measuring the drop in chloride concentration in the cathodic solution. Castellote et al. [25] have established a linear relationship between the chloride concentration and conductivity in the anodic compartment from the migration test, and pointed out that the diffusion coefficient can be calculated without making a chloride analysis but through the simple monitoring of the conductivity of the anolyte. Using the steady-state migration testing, Tong and GjØrv [26] established that the chloride diffusivities from steady-state, non-steady-state, and electrical conductivity measurements were well correlated. For concrete without mineral additives, measurements of initial electrical conductivity appear to provide a good basis for estimation of chloride diffusivity [26].

In this study, the first purpose is to determine if there exists a direct relationship between the steady-state and non-steady-state migration coefficient obtained from the accelerated chloride migration test. The second purpose is to determine if there is a relationship between the capillary pore volume and critical pore diameter and the transport properties (steady-state and non-steady-state migration coefficient).

2. Experimental program

2.1. Materials and specimen preparation

ASTM Type I Portland cement without mineral additions was used as binders. For concrete, river sand was used as fine aggregate and crushed limestone with a maximum size of 10 mm was used as coarse aggregate. In order to consider the same mortars in concrete and without taking into account the contribution of coarse aggregate, the mortar for the MIP was obtained from the fresh concrete passing a #4 (4.75 mm) sieve. In this study, eight w/c ratios ranging from 0.3 to 0.65, were selected in the mix proportions as shown in Table 1. For all mixes, the fine aggregate and coarse aggregate were constants as 865.1 and 811.5 kg/m^3, respectively. The dosage of superplasticizer (SP) was used for low w/c mixes (C30, C35, and C40) to attain the required workability (slump between 8 and 10 cm).

For each mix, a number of cylindrical specimens (ϕ 100×200 mm) were cast and cured. After mixing, a vibrating table was used to ensure good compaction. The surface of the specimens was then smoothed, and wet burlap was used to cover the concrete. After demolding, the specimens were cured in water (23 °C) for 28 days. The samples for the MIP tests were extracted from the center of the cylindrical specimens (mortar) using a core catcher. The resulting cylinder (ϕ 10×200 mm) was then cut with a fine saw to obtain the central cylinders with dimensions of ϕ 10×10 mm, and the ACMT specimen (30 mm in thickness) was obtained by sawing the mid-portion of concrete cylindrical specimen (ϕ 100×200 mm).

Table 1
Mix design

Mix	W/c	Unit content: kg/m^3				
		Water	Cement	Fine aggregate	Coarse aggregate	SP
C30	0.30	160	551	865	812	6
C35	0.35	173	510	865	812	5
C40	0.40	187	474	865	812	2
C45	0.45	199	443	865	812	0
C50	0.50	208	416	865	812	0
C55	0.55	216	392	865	812	0
C60	0.60	222	371	865	812	0
C65	0.65	228	351	865	812	0

2.2. Experimental procedure

2.2.1. Mercury intrusion porosimetry (MIP)

Before the test, the samples were dried by putting them in an oven at T=70 °C for 24 h or more to a constant weight and stored in sealed containers for the MIP test. The MIP test was carried out on a Micromeritics AutoPore-9520 mercury intrusion porosimeter capable of generating pressure in the range of subambient to 414 MPa (60,000 psi). The samples were evacuated to about 20 μm Hg and the low pressure was generated up to 30 psi by nitrogen gas. As the pressure on the mercury gradually increases, mercury is forced into the pores on the surface of the sample. Pressure was subsequently increased, in which equilibration is to be based on 10 s elapsed time at high pressure analysis. After each pressure increment, the equipment allowed the pressure and volume reading to stabilize before recording the pressure/volume data pair, until the maximum pressure 414 MPa was reached.

2.2.2. Accelerated chloride migration test (ACMT)

In order to avoid heterogeneity, the specimens were vacuum-saturated prior to test. Before the test, the lateral surface of the specimen was coated with epoxy and the specimen was placed in the vacuum desiccator, the pressure less than 1 mm Hg (133 MPa) was maintained for 3 h. De-aerated water was added to immerse the specimen and the vacuum level was maintained for one additional hour. Specimens were soaked in the added water for 18 h after turning off the pump.

The ACMT was used and described in Refs. [27,28]. The 30 mm thick slice was placed between two acrylic cells. One of the cells was filled with a 0.30 N NaOH solution and the other cell was filled with 0.52 N NaCl solution. The cells were

connected to a 24 V power source in which the NaOH electrode becomes the anode and the NaCl electrode becomes the cathode. During the test, the chloride ion concentration was determined from the solution in the anode cell, titrated with the $AgNO_3$ solution by the potentiometric titration method in accordance with AASHTO T260-97.

3. Results and discussion

3.1. The pore characteristic of mortars from the MIP

The porosity and pore size distribution study was carried out on the MIP. The cumulative intruded pore volume curves that obtained from the MIP for mortars with different w/c ratios are provided in Fig. 1. Although the samples were prepared with eight different w/c ratios, in the interests of clarity, only four distributions are given in Fig. 1. The remaining distributions fall between their appropriate neighbors in the plot. Each curve shown is the average of five separate tests. The pressures were converted to equivalent pore widths using the Washburn equation, as in Eq. (1):

$$d = \frac{-4\gamma \mathrm{Cos}\theta}{P}, \tag{1}$$

where d is the pore width, P is the net pressure across the mercury meniscus at the time of the cumulative intrusion measurement, γ is the surface tension, and θ is the contact angle between mercury and the pore wall. The values for γ and θ were assumed to be 0.484 N/m and 117°, respectively [29]. The values of pore size obtained from Eq. (1) are also shown in Fig. 1. This figure indicates that the total intruded volume of mercury per gram of the sample increases with increasing w/c ratio. For all mixes, the cumulative intruded mercury for pores larger than 500 nm shows almost no difference, but at the pore size between 150 and 50 nm the intruded mercury is significantly increased. The total intrusion volume of mercury obtained from the MIP for all specimens is shown in Table 2.

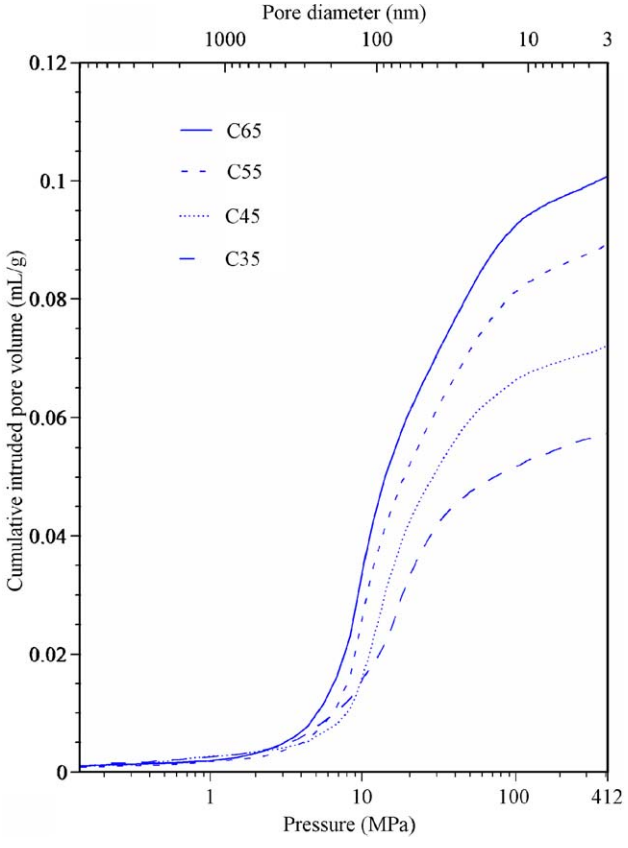

Fig. 1. The cumulative intruded pore volume of Hg curves obtained from the MIP.

Table 2
The total intrusion volume and capillary pore volume of Hg, and critical pore diameter for mortar

Mix	Total intrusion volume (mL/g)		Capillary pore volume (30–10,000 nm), (mL/g)		Critical pore diameter (nm)	
		Average		Average		Average
C30	0.0588	0.0528	0.0465	0.0427	77	77
	0.0535		0.0416		82	
	0.0587		0.0459		74	
	0.0454		0.0403		79	
	0.0476		0.0391		74	
C35	0.0545	0.0580	0.0427	0.0445	85	77
	0.0604		0.0433		81	
	0.0591		0.0476		75	
	0.0561		0.0433		72	
	0.0599		0.0455		74	
C40	0.0666	0.0684	0.0585	0.0542	83	84
	0.0701		0.0551		86	
	0.0696		0.0531		84	
	0.0680		0.0523		82	
	0.0675		0.0519		87	
C45	0.0715	0.0707	0.0559	0.0547	99	106
	0.0700		0.0554		110	
	0.0713		0.0536		107	
	0.0694		0.0540		104	
	0.0715		0.0545		107	
C50	0.0873	0.0829	0.0758	0.0627	125	117
	0.0772		0.0553		104	
	0.0887		0.0631		118	
	0.0821		0.0637		120	
	0.0790		0.0558		117	
C55	0.0917	0.0883	0.0689	0.0654	139	130
	0.0889		0.0649		120	
	0.0876		0.0656		119	
	0.0872		0.0643		138	
	0.0861		0.0635		134	
C60	0.0921	0.0901	0.0797	0.0723	136	134
	0.0886		0.0633		146	
	0.0881		0.0624		140	
	0.0910		0.0786		129	
	0.0906		0.0775		122	
C65	0.1043	0.1022	0.0763	0.0772	130	142
	0.1032		0.0780		149	
	0.1057		0.0886		148	
	0.0988		0.0688		158	
	0.0992		0.0742		126	

The volumes of mercury intrusion in a specified range of pores were normalized by the total volume of mercury intrusion of the same specimen. To appreciate the distribution of pores, the normalized volume of mercury intrusion belonging to the

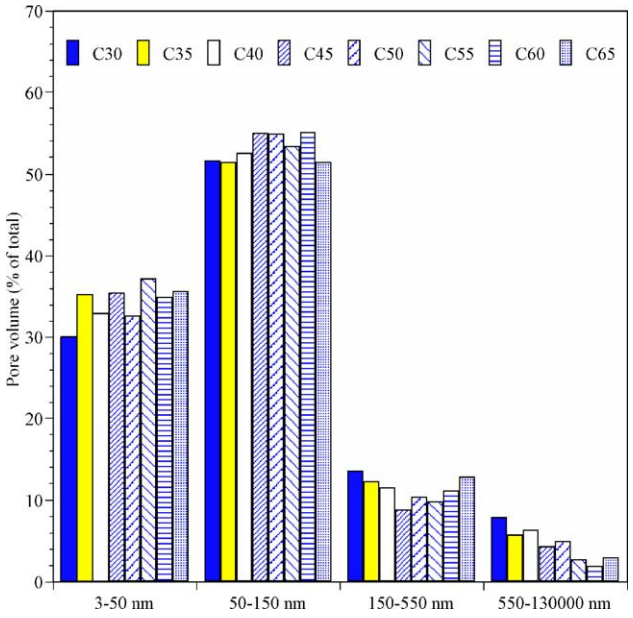

Fig. 2. Pore size distribution of mortars with different w/c ratios.

pore width ranges greater than 550, 150–550, 50–150, and 3–50 nm was calculated from these intrusion curves, and these results are shown in Fig. 2. The mortars with different w/c ratio show a very similar normalized volume of mercury intrusion in all pore width ranges. There was a large penetration of mercury in the pore range of 3 to 50 nm and 50 to 150 nm. For all mixes, the trend of pore size distribution was similar.

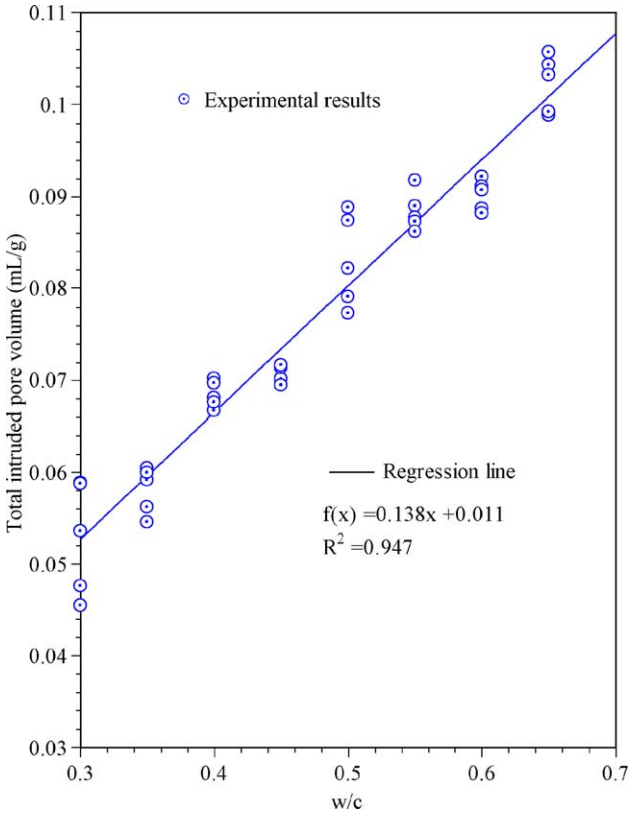

Fig. 3. Correlation between total intruded pore volume and w/c.

Fig. 3 shows the relationship between the total intrusion volume of mercury obtained from the MIP and the w/c ratio for all mixes, and the corresponding regression results are also shown in this figure. It can be seen in Fig. 3, that a linear relationship exists between the total intrusion volume of mercury and w/c, with a regression coefficient R^2 of 0.947.

3.2. Chloride migration in the ACMT

Studying the chloride–time curve obtained from the ACMT of concrete is a way to understand the permeability of these materials. In this study, the chloride concentration was determined from the solution in the anode cell and was the average of three individual results. The typical result of chloride concentration is plotted in Fig. 4(a) as a function of time. Fig. 4 (a) shows that three stages exist, non-steady-state, transition period, and steady-state with respect to the change of the chloride concentration. In the non-steady-state, the chloride ions are in the process of migrating through saturated pores in concrete and have not yet reached the anode cell. In the transition period between points A and B in Fig. 4(a) and (b), the first chloride ions penetrate through the specimen, and there is an uneven distribution of the chloride content in the specimen [26]. In the steady-state, the flux of chloride ions passing through the concrete specimen becomes constant.

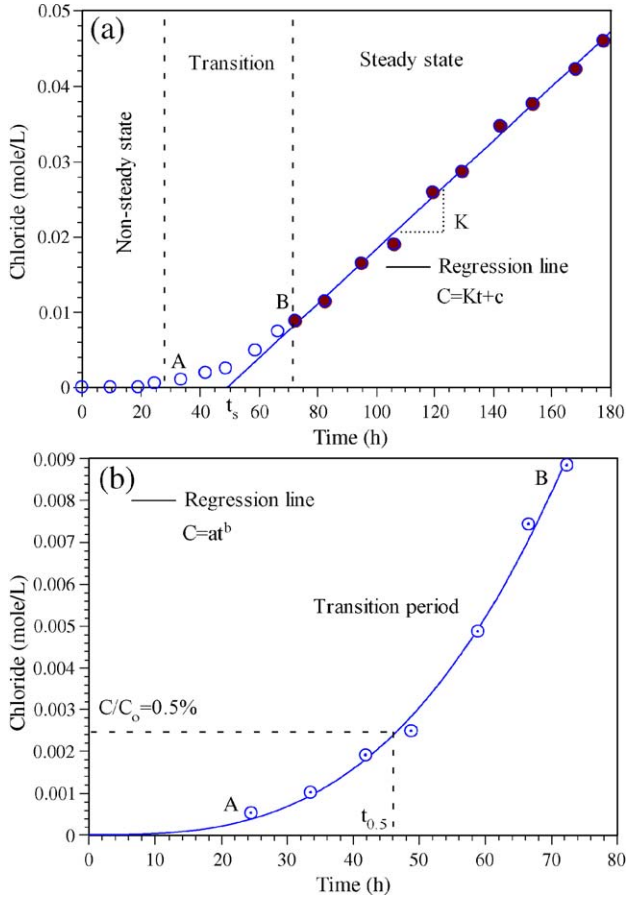

Fig. 4. Variations of chloride concentration (a), and in transition period (b).

In the non-steady-state condition, the chloride ions have not yet reached the anode cell. The non-steady-state diffusion coefficient is determined based on measurements of the time-span for chloride ion penetration through specimen when the chloride ion reaches the edge of the anode cell. Since the chloride concentration is not continually monitored and the time-span is not easy to determine, a regression line is carried out for the transition period portion of the chloride–time curve to determine the time-span for chloride ion penetration through specimen as:

$$C = at^b, \qquad \text{for transition period} \tag{2}$$

where C is the chloride concentration in anode cell, t is the elapsed time, a and b are the experimental constants. The time $t_{0.5}$ corresponding to C/C_0=0.5% (C/C_0, chloride concentration in anode cell/chloride concentration in source cell) [11] was calculated from Eq. (2), and listed in Table 3.

In the steady-state, to calculate the chloride migration rate (K) for chloride ion penetration, linear regression is carried out for the steady-state portion of the curve as:

$$C = Kt + c, \qquad \text{for steady state} \tag{3}$$

where K (chloride migration rate) is the slope of the chloride–time curve for the steady-state portion. The time t_s, $t_s = -c/K$, determined by the interception of the steady-state chloride–time curve and the time axis is the time-span for chloride ion penetration through specimen from the steady-state as shown in Fig. 4(a). The values of t_s and K for all specimens are listed in Table 3.

Table 3
Breakthrough time from steady-state and non-steady-state conditions, and the chloride migration rate

Mix	$t_{0.5}$ (h)	t_s (h)	K (mol/L/h × 10^{-4})
C30	56.58	49.78	3.61
	47.89	40.02	3.46
	47.58	49.78	3.61
C35	35.65	34.70	5.11
	34.06	35.64	4.96
	37.81	36.98	4.61
C40	28.01	28.97	6.60
	32.68	20.73	5.47
	32.79	30.19	5.86
C45	25.77	20.72	6.52
	27.58	26.50	6.28
	26.70	24.63	5.80
C50	16.57	16.34	9.44
	18.54	17.74	9.02
	19.52	20.03	8.83
C55	15.32	13.85	10.56
	14.92	10.09	10.40
	13.96	14.04	11.27
C60	15.24	13.74	10.39
	12.41	11.82	11.83
	14.47	15.02	12.28
C65	12.15	11.89	13.76
	12.81	12.70	13.21
	12.38	13.98	13.57

Table 4
The non-steady-state migration coefficients M_{n5} and M_{ns} obtained from $t_{0.5}$ and t_s, and the steady-state migration coefficient M_s

Mix	M_{n5}, ($m^2/s \times 10^{-12}$)		M_{n5}		M_s, ($m^2/s \times 10^{-12}$)	
		Average				Average
C30	4.14	4.65	4.70	5.08	3.52	3.48
	4.89		5.82		3.38	
	4.92		4.70		3.52	
C35	6.57	6.54	6.75	6.55	4.98	4.77
	6.87		6.57		4.84	
	6.19		6.33		4.50	
C40	8.36	7.55	8.08	9.04	6.44	5.83
	7.16		11.29		5.34	
	7.14		7.76		5.72	
C45	9.08	8.78	11.30	9.88	6.36	6.05
	8.49		8.83		6.12	
	8.77		9.50		5.66	
C50	14.13	12.92	14.33	13.07	9.21	8.87
	12.63		13.20		8.80	
	11.99		11.69		8.61	
C55	15.28	15.91	16.91	18.93	10.30	10.48
	15.69		23.20		10.14	
	16.78		16.68		11.00	
C60	15.36	16.80	17.04	17.48	10.14	11.22
	18.86		19.80		11.54	
	16.18		15.59		11.98	
C65	19.27	18.82	19.69	18.29	13.43	13.19
	18.28		18.44		12.89	
	18.91		16.74		13.24	

3.3. Chloride migration coefficient

In the ACMT, chloride ions are transported in concrete under an applied voltage. The non-steady-state migration coefficient obtained from the ACMT in non-steady-state can be calculated from the modified Fick's second law. From the analytical solution of the modified Fick's second law, the non-steady-state migration coefficient can be calculated as [11]:

$$M_n = \frac{1}{\beta}\left[\frac{x - \alpha\sqrt{x}}{t}\right], \tag{4}$$

where $\beta = \frac{|z|FE}{RT}$, $\alpha = 2\sqrt{\frac{1}{\beta}}\mathrm{erf}^{-1}\left(1 - \frac{2C}{C_o}\right)$, M_n is non-steady-state migration coefficient in m^2/s, z is the electrical charge of chloride, F is the Faraday constant (96500 C/mol), E is the strength of the electric field between the anode and cathode (V/m), R is the universal gas constant (8.3 J/mol/K), T is absolute temperature (K), C is chloride concentration in the anode cell (mol/L), C_o is chloride concentration in the source cell (mol/L) and erf^{-1} is the inverse of error function. By using the time $t_{0.5}$ and t_s in Table 3, the non-steady-state migration coefficients M_{n5} and M_{ns}, respectively, are calculated from Eq. (4). The non-steady-state migration coefficients M_{n5} and M_{ns} obtained from $t_{0.5}$ and t_s for all specimens are listed in Table 4.

In the steady-state, using the Nernst–Planck's equation that the steady-state migration coefficient, M_s, is calculated as [16]:

$$M_s = \frac{RT}{|z|C_oFE}\frac{V_aK}{A}, \tag{5}$$

where V_a is the volume of solution in anode cell (m^3), and A is the specimen surface exposed to chloride ions (m^2). By using the chloride migration rate (K) in Table 3 and Eq. (5), the steady-state migration coefficient (M_s) for all specimens is calculated, and listed in Table 4.

A comparison of the steady-state migration coefficient (M_s) based on the steady-state and the non-steady-state migration coefficient obtained on the basis of different breakthrough times ($t_{0.5}$ and t_s in Table 3) are demonstrated in Fig. 5(a) and (b). From Fig. 5(a), it can be seen that a well correlated linear relationship between the non-steady-state migration coefficient (M_{n5}) obtained on the basis of $t_{0.5}$ and the steady-state migration coefficient (M_s) was observed. Comparing the regression results in Fig. 5(a) and (b), it can be obtained that the linearity between M_{n5} and M_s is better than M_{ns} (the non-steady-state migration coefficient obtained on the basis of t_s) and M_s.

3.4. Capillary pore volume, critical pore diameter, and migration diffusivity

As previously mentioned, Portland cement-based material is a porous construction material. The capillary porosity and connectivity of these capillary pores are the most important characteristics of pore system related to the diffusivity of concrete. Since the critical pore diameter represents the grouping of the largest fraction of interconnected pores influencing the transport properties [11], the critical pore diameter can be used to assess the connectivity of cement-based

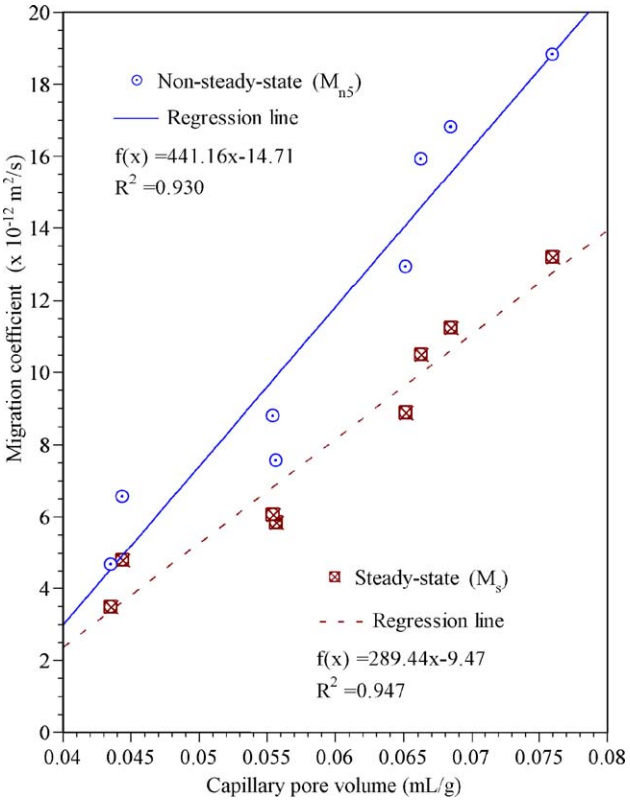

Fig. 6. Capillary pore volume vs. the non-steady-state migration coefficient obtained on the basis of $t_{0.5}$ and the steady-state migration coefficient.

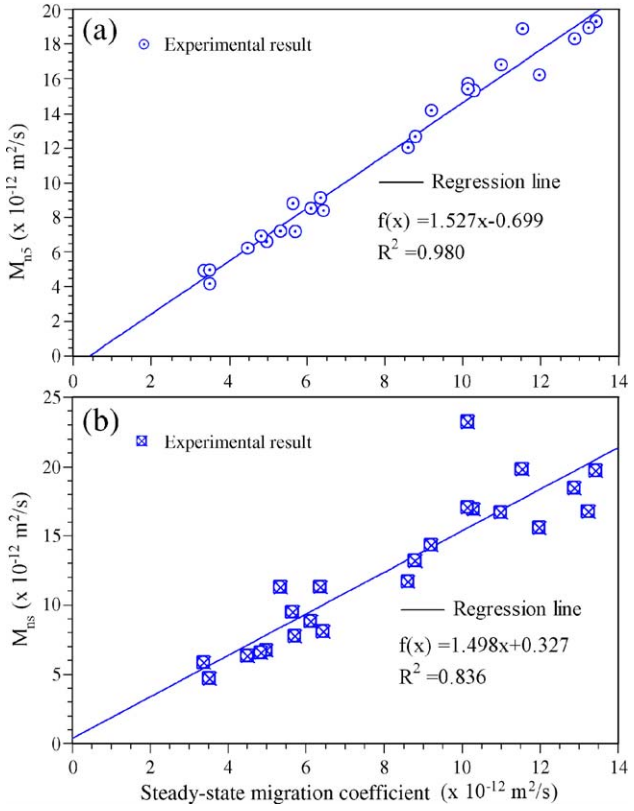

Fig. 5. Correlation between the steady-state migration coefficient and non-steady-state migration coefficient obtained on the basis of $t_{0.5}$ (a), and t_s (b).

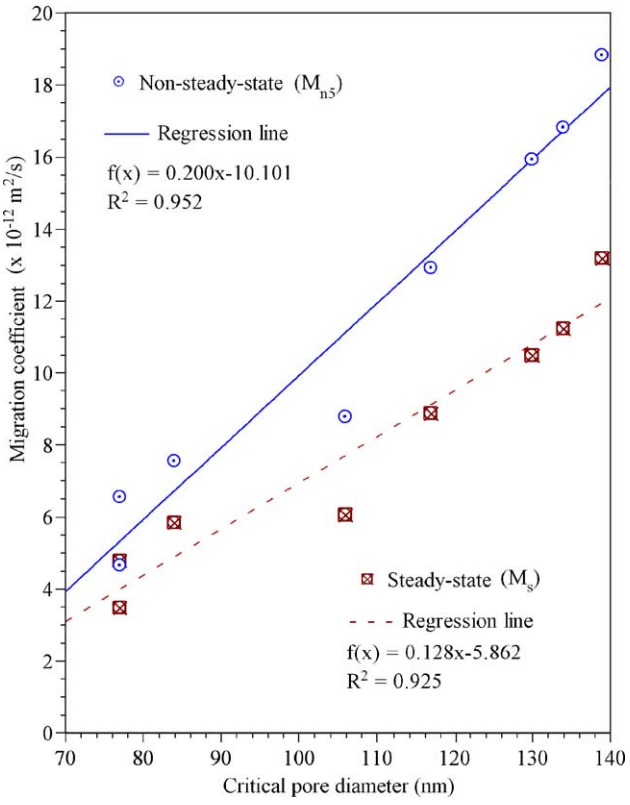

Fig. 7. Critical pore diameter vs. the non-steady-state migration coefficient obtained on the basis of $t_{0.5}$ and the steady-state migration coefficient.

materials. The critical pore diameter (d_c) is defined as the inflection point on the intrusion pore volume (V) versus diameter (d) curve, or the maximum of the dV/(log d) curve. The results of the capillary pore volume (pore diameter between 30 to 10,000 nm) and the critical pore diameter for all mixtures are listed in Table 2.

The migration coefficients of non-steady-state and steady-state, determined from the ACMT, are plotted against the capillary pore volume obtained from the MIP in Fig. 6. Each ACMT and the MIP result shown is the average of three and five separate tests, respectively. The data in Fig. 6 was also carried out by the linear regression analysis, from which indicates that the steady-state migration coefficient, non-steady-state migration coefficient, and the capillary pore volume are linearly correlated. Fig. 7 illustrates the relationship between the critical pore diameter, determined from the MIP, and migration coefficients of steady-state and non-steady-state obtained from the ACMT. The linear relationship between the critical pore diameter and steady-state migration coefficient as well as the critical pore diameter and non-steady-state migration coefficient are fairly good. It appears that capillary porosity and connectivity of those pores are important characteristics of pore system related to the diffusivity of chloride ions in ordinary Portland cement concrete.

4. Conclusions

The chloride migration in free mineral addition concrete with the constant aggregates was investigated using the ACMT, and the pore characteristic of the same mortars in concrete was obtained from the MIP. The non-steady-state and steady-state migration coefficients were calculated from the modified Fick's law. Based on the results obtained from the present experimental investigation, the following conclusions can be drawn.

(1) The reported migration coefficients show good linearity between steady-state and non-steady-state accelerated chloride migration tests, since the same experimental setup and specimen were used, and a linear variation of the electrical potential in the specimen was assumed to calculate the migration coefficient of steady-state and non-steady-state. But, the migration coefficient of non-steady-state is higher than the steady-state. It is possible that a part of chloride ions bound to the hydration products, and block some fine pores in steady-state, and reduced the steady-state migration coefficient. The different time to reach non-steady-state and steady-state do not affect the correlation between the migration coefficients of steady-state and non-steady-state.

(2) Because the chloride–time curve in the transitional period is non-linear, the linearity between the steady-state migration coefficient (M_s) and M_{n5} (obtained from $t_{0.5}$ in Fig. 4) is better than M_s and M_{ns} (obtained from t_s in Fig. 4).

(3) The migration coefficients are linearly related to the capillary pore volume (pore diameter between 30 to 10,000 nm) and the critical pore diameter. In the migration test, chloride ions migrate through the pore solution in concrete. The critical pore diameter represents the grouping of the largest fraction of interconnected pores in the specimens. The chloride migration coefficients are influenced by the capillary pore volume and the connectivity of pores in the specimens.

Acknowledgment

The financial support of the National Science Council, ROC, under grant NSC 93-2211-E-019-017 is gratefully appreciated.

References

[1] H.R. Samaha, K.C. Hover, Influence of microcracking on the mass transport properties of concrete, ACI Mater. J. 89 (4) (1992) 416–424.
[2] P.K. Mehta, P.J.M. Monteiro, Concrete: Structure, Properties, and Materials, Prentice Hall, New Jersey, 1993.
[3] V.T. Ngala, C.L. Page, L.J. Parrott, S.W. Yu, Diffusion in cementitious materials: II. Further investigations of chloride and oxygen diffusion in well-cured OPC and pastes, Cem. Concr. Res. 25 (4) (1995) 819–826.
[4] H. Uchikawa, S. Hanehara, H. Hirao, Influence of microstructure on the physical properties of concrete prepared by substituting mineral powder for part of fine aggregate, Cem. Concr. Res. 26 (1) (1996) 101–111.
[5] C. Shi, Strength, pore structure and permeability of alkali-activated slag mortars, Cem. Concr. Res. 26 (12) (1996) 1789–1799.
[6] L. Jiang, Y. Guan, Pore structure and its effect on strength of high-volume fly ash paste, Cem. Concr. Res. 29 (4) (1999) 631–633.
[7] S.P. Pandey, R.L. Sharma, The influence of mineral additives on the strength and porosity of OPC mortar, Cem. Concr. Res. 30 (1) (2000) 19–23.
[8] M. Frias, J. Cabrera, Pore size distribution and degree of hydration of metakaolin-cement pastes, Cem. Concr. Res. 30 (4) (2000) 561–569.
[9] T. Matusinovic, J. Sipusic, N. Vrbos, Porosity–strength relation in calcium aluminate cement pastes, Cem. Concr. Res. 33 (11) (2003) 1801–1806.
[10] V.T. Ngala, C.L. Page, Effect of carbonation on pore structure and diffusional properties of hydrated cement paste, Cem. Concr. Res. 27 (7) (1997) 995–1007.
[11] P. Halamickova, R.J. Detwiler, D.P. Bentz, E.J. Garboczi, Water permeability and chloride ion diffusion in Portland cement mortars: relationship to sand content and critical pore diameter, Cem. Concr. Res. 25 (4) (1995) 790–802.
[12] S. Diamond, Mercury porosimetry an inappropriate method for the measurement of pore size distributions in cement-based materials, Cem. Concr. Res. 30 (10) (2000) 1517–1525.
[13] K.L. Willis, A.B. Abell, D.A. Lange, Image-based characterization of cement pore structure using wood's metal intrusion, Cem. Concr. Res. 28 (12) (1998) 1695–1705.
[14] S. Diamond, J. Huang, The ITZ in concrete—a different view based on image analysis and SEM observations, Cem. Concr. Com. 23 (2–3) (2001) 179–188.
[15] Standard test method for electrical indication of concrete's ability to resist chloride ion penetration, ASTM C 1202-97, American Society for Testing and Materials, 1994.
[16] C. Andrade, Calculation of chloride diffusion coefficients in concrete from ionic migration measurements, Cem. Concr. Res. 23 (3) (1993) 724–742.
[17] T. Zhang, O.E. Gjørv, An electrochemical method for accelerated testing of chloride diffusivity in concrete, Cem. Concr. Res. 24 (8) (1994) 1534–1548.
[18] C.C. Yang, S.W. Cho, R. Huang, The relationship between charge passed and the chloride-ion concentration in concrete using steady-state chloride migration test, Cem. Concr. Res. 32 (2) (2002) 217–222.
[19] L. Tang, L. Nilsson, Rapid determination of the chloride diffusivity in concrete by applying an electrical field, ACI Mater. J. 89 (1) (1992) 49–53.

[20] D. Whiting, Rapid measurements of chloride permeability of concrete, Public Roads 45 (3) (1981) 101–112.
[21] R.F. Feldman, G.W. Chan, R.J. Brousseau, P.J. Tumidajski, Investigation of the chloride permeability test, ACI Mater. J. 91 (2) (1994) 246–255.
[22] R.F. Feldman, L.R. Prudencio Jr., G. Chan, Rapid chloride permeability test on blended cement and other concretes: correlations between charge, initial current and conductivity, Constr. Build. Mat. 13 (3) (1999) 149–154.
[23] T. Sugiyama, Y. Tsuji, T.W. Bremner, Relationship between coulomb and migration coefficient of chloride ions for concrete in a steady-state chloride migration test, Mag. Concr. Res. 53 (1) (2001) 13–24.
[24] O. Truc, J.P. Ollivier, M. Carcasses, A new way for determining the chloride diffusion coefficient in concrete from steady state migration test, Cem. Concr. Res. 30 (7) (2000) 217–226.
[25] M. Castellote, C. Andrade, C. Alonso, Measurement of the steady and non-steady-state chloride diffusion coefficients in a migration test by means of monitoring the conductivity in the anolyte chamber comparison with natural diffusion tests, Cem. Concr. Res. 31 (10) (2001) 1411–1420.
[26] L. Tong, O.E. GjØrv, Chloride diffusivity based on migration testing, Cem. Concr. Res. 31 (7) (2001) 973–982.
[27] C.C. Yang, The relationship between migration coefficient of chloride ions for concrete and charge passed in steady state using the accelerated chloride migration test, ACI Mater. J. 101 (2) (2004) 124–130.
[28] C.C. Yang, S.W. Cho, The relationship between chloride migration rate for concrete and electrical current in steady state using the accelerated chloride migration test, Mater. Struct. 37 (271) (2004) 456–463.
[29] R. Kumar, B. Bhattacharjee, Study on some factors affecting the results in the use of MIP method in concrete research, Cem. Concr. Res. 33 (3) (2003) 417–424.